JOURNAL OF CATALYSIS 144, 311–324 (1993)

XAFS Characterization of Rh/Al_2O_3 after Treatment in High-Temperature Oxidizing Environments

D. D. BECK,* T. W. CAPEHART,† C. WONG,* AND D. N. BELTON*

*Physical Chemistry Department and †Physics Department, General Motors Research, 30500 Mound Rd., Box 9055, Warren, 48090-9055 Michigan

Received June 17, 1991; revised April 20, 1993

The effect of high-temperature oxygen aging on the local structure of Rh oxide particles in a Rh/Al_2O_3 catalyst has been characterized using X-ray absorption fine structure (XAFS) measurements. Thermal aging of the catalyst was performed at various temperatures and for different lengths of time at selected temperatures. Following treatment in 5% oxygen at or above 500°C, the supported Rh is completely oxidized to orthorhombic Rh_2O_3. The coordination of the dominant shells in the radial distribution function increases with treatment temperature, reaching a maximum at 800°C. Above this treatment temperature, the coordination in these shells decreases dramatically with increasing treatment temperature. Treatment in 5% oxygen at temperatures near 800°C for an extended period results in an increase in coordination of the first three dominant shells. Most of this increase takes place during the initial 1–2 h of treatment, but proceeds more slowly thereafter. Extended treatment at lower temperatures (600°C) results in slow and gradually increasing coordination in these shells, while at much higher temperatures (1000°C) the coordination initially increases but then decreases over extended treatment periods. The latter behavior is coincident with an apparent change in the structure as well. Since XAFS provides insight about single crystallite domains, the results suggest that at 800°C, Rh_2O_3 crystallite growth or consolidation is more favored than at lower or higher temperatures. The behavior of the supported Rh_2O_3 at high temperatures indicates a strong interaction with the support; however, this interaction does not appear to involve formation of a spinel or dissolution of Rh cations into the alumina lattice. Alternative explanations for these observations are discussed.

INTRODUCTION

In automotive emission control catalysts, the efficient use of the noble metals is desirable because of their limited supply and high cost. This is particularly true of the Rh component, which plays an important role in the reduction of nitrogen oxides as well as the oxidation of hydrocarbons and carbon monoxide (*1–3*). Unfortunately, the operation of three-way catalysts at elevated temperatures causes a variety of changes in the character of the supported metal, which generally leads to loss of catalytic activity (*4, 5*). Thus, the understanding of the process involved in thermal degradation of the catalyst is important and has been the subject of numerous studies of the behavior and mechanisms involved in thermal aging of catalysts (*4–7*).

Some knowledge concerning the behavior of Rh/Al_2O_3 in high-temperature environments has been gained from previous studies. When Rh/Al_2O_3 is thermally aged in a reducing environment, Rh metal particles generally sinter, resulting in a loss of metal surface area available for catalytic reaction sites (*4, 6, 7*). Thermal aging of Rh/Al_2O_3 in an oxidizing environment causes not only the oxidation of supported Rh particles (*2, 8–10*), but at relatively high temperature also results in the formation of an oxidized form of Rh which is subsequently difficult to reduce to the metal (*11–16*), and hence difficult to reactivate. In contrast, Rh_2O_3 can be easily reduced to Rh metal in a reducing environment at 200°C (*17, 18*). This aspect of the behavior of supported Rh has been the subject of a number of studies (*10–17, 19–25*), and several mechanisms have been

0021-9517/93 $5.00

proposed to explain this behavior. One of these mechanisms involves the formation of an oxide of Rh on the surface of the support which as yet to be structurally characterized, but is unlike the known forms of Rh_2O_3 or RhO_2 (*23*). An alternate mechanism involves a strong interaction between the metal and the support which results in the formation of two dimensional Rh oxide moieties (*15*), or even the formation of a spinel on the surface or within the bulk of the support lattice (*22, 24*). These mechanisms have been suggested on the basis of chemisorption and activity measurements, but not from more direct structural analysis. These moieties appear to lack any significant domain size and are difficult to characterize using X-ray diffraction techniques, and have only recently been the focus of TEM studies. The XAFS technique has the unique ability to characterize the local structure in materials which consist of very small particles or domains (*25*), and thus can be used to gain a better understanding of the nature and structure of Rh/Al_2O_3 as a function of treatment in high-temperature environments. In this work, the local structure of Rh/Al_2O_3 thermally aged in an oxidizing environment was determined for a range of treatment temperatures (500 to 1100°C). For selected treatment temperatures, changes in the local structure of the supported Rh oxide were studied as a function of exposure time.

EXPERIMENTAL

Sample Preparation and Treatment

The 1 wt% Rh/Al_2O_3 catalyst lot used in this study was prepared in the following manner. First, 200 g of alumina spheres (W. R. Grace low bulk density alumina, 3.2 mm diameter, 100 m^2/g, 1.1 ml/g pore volume) were combined with a solution of 6.11 g $Rh(NH_3)_6Cl_3$ in 200 ml of water. The spheres were air dried overnight and then calcined in flowing air (460 cm^3/min) for 4 h at 500°C. This material was then ground into a powder and sieved using a 100 mesh sieve. The Rh dispersion of this catalyst was measured as 0.45 using chemisorption of H_2. Each of the catalyst samples was prepared in the following way prior to obtaining an X-ray absorption measurement. A 3-g sample was inserted in a 60-cm length of round quartz tubing having an outer diameter of 14 mm and a wall thickness of 1 mm. For one series of experiments, each sample was treated in 5% O_2/N_2 flowing at 50 sccm at a chosen temperature in the range of 500 to 1100°C for 2 h. At the end of the treatment, the sample was cooled in the gas flow to 25°C, and then the ends of the tube were sealed by collapsing and closing the glass tube quickly with a torch. Using this process, the treatment gas remains in the tube. Several samples were treated at one particular treatment temperature (500, 600, 800, and 1000°C), but for various times (1, 2, 4, and 15 h).

In addition to the catalyst samples, measurements were also obtained for selected chemical compounds of known structure. These compounds include Rh foil (25 μm thick), orthorhombic Rh_2O_3, and RhO_2, all obtained from Alfa. Two additional samples, untreated Rh black and Rh black treated in 5% O_2/N_2 at 900°C for 24 h, were also examined. The radial structure functions for each of these compounds appears in Fig. 1, while the known structural parameters obtained using crystallographic measurements are reviewed in Table 1. For each compound except the foil, a thin powder bed about 100 μm in thickness was prepared and sandwiched in Kapton tape. The identity and crystallinity of these compounds were confirmed using X-ray diffraction mesurements. Note that the radial structure functions obtatined by Fourier transforming the corresponding χ functions are shown without correction for phase shifting (corrections for phase shift were performed when the individual shells were analyzed). Therefore, the radial structure functions shown in the figures do not correspond to the actual radial distance.

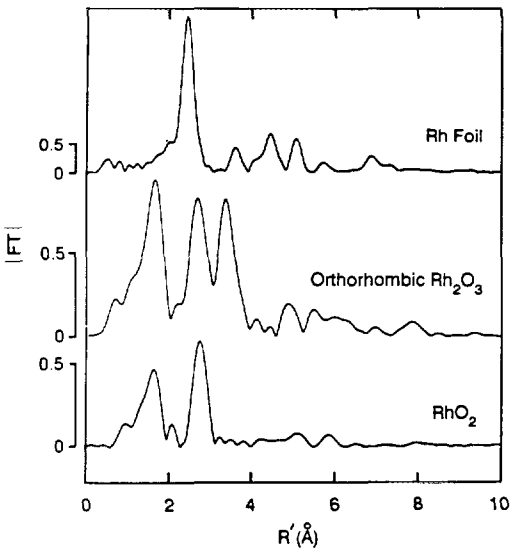

FIG. 1. Radial structure functions obtained for the Rh Foil, orthorhombic Rh_2O_3, and RhO_2 reference compounds. As noted in the text, the spectra as represented in this figure have not been corrected for phase shift.

X-Ray Absorption Measurements

Following treatment and sealing in the quartz tubes, the catalyst samples and reference compounds were transported to the National Synchrotron Light Source (NSLS) at Brookhaven National Laboratory for measurement of the x-ray absorption in the region of the Rh *K*-edge (23.160 to 25.040 keV). Measurements were obtained using beamline X-11A equipped with a two (Si(111) crystal monochromator which was detuned by 20% to suppress harmonic contributions to the spectra. For all measurements, the X-ray ring operated at an energy of 2.5 GeV and at a stored beam current in the range 40–120 mA. The Rh *K*-edge at 23.220 keV (*26*) obtained by absorption through the Rh foil was used to calibrate the monochromator. Measurements obtained with the other reference compounds and treated catalyst samples were then referenced to this calibration. All X-ray absorption spectra were obtained at 25°C using a transmission detection configuration. Apertures of 1 mm × 5 mm were positioned in front of the first detector (I_0), in front of the catalyst sample, and in front of the second detector (I). Detection of the X-ray flux was obtained using ion chamber detectors filled with Ar or Ar/N_2 mixtures (*27*). Prior to measurement, each of the sealed quartz sample tubes was placed on end and tapped such that the catalyst powder filled one end of the tube in a packed bed. The tube was then placed in a sample holder such that the long dimension of the beam cross-section (5 mm) was aligned with the center axis of the tube. Using this configuration, all of the X-ray photons that reach the second detector pass through a catalyst bed of relatively uniform thickness (12.0 ± 0.2 mm). Absorption spectra for the reference compounds were obtained by placing the sandwiched powders behind the aperture opening on the sample holder.

The method used to analyze the XAFS data is consistent with methods used by other researchers and is described as follows (*28, 29*). The absorption coefficient function $\mu(E)$, defined as $\ln(I_0/I)$, was ob-

TABLE 1

Reference Compound Structural Information

Compound	Shell	Interaction	*N*	*R* (Å), mean
Rh Foil[a]	1st	Rh(0)–Rh(0)	12	2.687
	2nd	Rh(0)–Rh(0)	6	3.80
	3rd	Rh(0)–Rh(0)	24	4.65
	4th	Rh(0)–Rh(0)	12	5.37
RhO_2[b]	1st	Rh(IV)–O	6	1.96
	2nd	Rh(IV)–Rh(IV)	8	na
Rh_2O_3 (hex)[c]	1st	Rh(III)–O	6	2.05
	2nd	Rh(III)–Rh(III)	4	2.95
Rh_2O_3(ortho)[d]	1st	Rh(III)–O	6	2.06
	2nd	Rh(III)–Rh(III)	4	3.03
	3rd	Rh(III)–Rh(III)	10	3.67

[a] Values determined from crystallography (*41*). Only the first four significant shells are listed.

[b] Calculated from reported RhO_2 lattice constants and space group (*32, 42*). Only the two most intense shells are listed. The Rh(IV)–Rh(IV) distance has not been reported.

[c] Values determined from crystallography (*43–45*). Only the most intense shells are listed, and the radial distance represents a mean of a distribution of scattering distances.

[d] Values determined from crystallography (*44–46*). Only the three most intense shells are listed, and the radial distances shown represent a mean of a distribution of scattering distances.

tained and a preliminary background was removed by least-squares spline fitting a quadratic background function to $\mu(E)$. The edge jumps were then normalized to unity and a final background was estimated using a polynomial fit in k-space. This resulting $\chi(k)$ function was then k^2 weighted to emphasize the signal of interest and Fourier transformed over the largest possible range in k-space ($\Delta k \sim 2.3$–20.0 Å^{-1} for Rh_2O_3 and RhO_2, $\Delta k \sim 2.17$–22.0 Å^{-1} for Rh foil, and $\Delta k \sim 2.3$–20.0 Å^{-1} for the catalyst samples) to produce the raw radial structure function, $|\rho(r)|$. Each limit in k-space was chosen at a node in the XAFS spectrum.

The XAFS spectra were analyzed using experimentally obtained phase shift functions and backscattering amplitudes from reference compounds. The structural parameters associated with each shell in the reference compounds were obtained from crystallographic data (Table 1). The nearest neighbor shells in the catalyst samples were relatively well resolved and identified with scattering from the nearest oxygen anion shell surrounding the Rh cation scatterer. These shells were analyzed by first filtering and inverse transforming the peak of interest in the $|\rho(r)|$ function using limits which coincide with nodes in the imaginary part of the Fourier transform function (typically in the range of 1.11 to 2.01 Å for the first shell (oxygen anions), 2.36 to 3.05 Å for the second shell (Rh cations), and 3.05 to 3.81 Å for the third shell (Rh cations), then least-squares fitting the corresponding $\chi(k)$ function derived from the same coordination shell in the reference compound (*26*). For consistency, the phase and amplitude functions obtained from the reference compounds were compared with those generated by McKale *et al.* using curved wave models for scatterers of the same identity (*30*). The crystallographic data for the oxides of Rh reflect the characteristic asymmetry of their structures, thus a given shell typically consists of a distribution of scattering distances. However, the structure of the Rh oxide in the catalyst samples was characterized by a relatively narrow distribution of scattering distances in a particular shell; thus, their structures were more symmetric than bulk Rh_2O_3. For the purpose of this study, then, we found that choosing a single "mean" distance in fitting these shells produced satisfactory fits to the χ functions, with consistently negative Debye–Waller terms, again indictive of greater symmetry in the Rh oxide structures in the catalyst samples. Higher order shells in the catalysts were also assumed to contain overlapping contributions from both Rh cation and oxygen anion scatterers. Therefore, we combined contributions from Rh and O amplitude and phase functions (heavily weighted in the Rh contribution) and allowed the amplitudes, phases, and relative contributions to vary to obtain a least-squares fit to the χ function for these two shells. The best fit always contained a relatively small contribution from oxygen (less than 15% in the 2nd dominant shell, and less than 8% in the third dominant shell) which was expected since oxygen is a much weaker scatterer than Rh at these distances. We found that the inclusion of oxygen improved the fit to the χ function only in the region of low k values, which is consistent with the maximum in the amplitude function of oxygen at ~3 Å^{-1}. However, when these shells were fit using only a contribution from Rh, the quality of the best fit to the χ functions was only marginally worse, and the resulting coordination and radii information were not significantly affected. For consistency, then, we used only contributions from Rh amplitude and phase functions in fitting these higher order shells, and chose the best fit to $\chi(k)$ in the region above 6 Å^{-1}.

In all of the radial structure functions obtained for the oxidized catalyst samples, a low frequency component was present in the absorption spectra which gives rise to a peak in the corresponding radial structure functions occurring at an unusually low radius. Although the phase and amplitude functions of this feature were similar to an oxygen anion, the best fit produces a radial

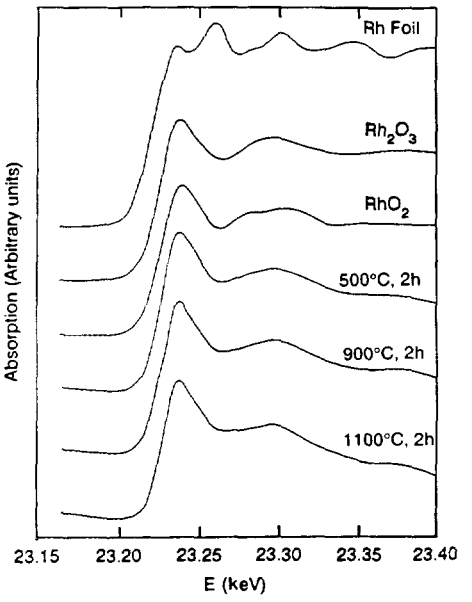

FIG. 2. The near-edge spectra obtained for Rh foil, orthorhombic Rh_2O_3, RhO_2, and catalyst samples treated at 500, 900, and 1100°C.

distance which is too small (<1.5 Å, apparent) to be rationalized as a physical shell involving Rh(III) and oxygen. This feature is usually well resolved from the dominant oxygen anion shell and for the purpose of this study is taken to be an artifact from residual background.

RESULTS AND DISCUSSION

In the first part of this work, the effect of aging the 1 wt% Rh/Al_2O_3 catalyst in 5% O_2/N_2 at a variety of temperatures was investigated. The near-edge X-ray absorption spectra (23.16 to 23.40 keV) obtained for Rh/Al_2O_3 catalyst samples treated at 500, 900, and 1100°C are compared with near-edge spectra obtained for Rh foil, orthorhombic Rh_2O_3 and RhO_2 in Fig. 2. Note that the near-edge structures of the treated catalyst samples are more like that of the Rh_2O_3 reference compound than that of RhO_2 or the Rh metal. This comparison was performed in a more quantitative manner by fitting the near edge spectra to the sum of the standard formula $(1/\pi)\tan^{-1}[2(E-\varepsilon_L)/\delta]$, which assumes a constant density of final states and matrix elements, and Lorentzian functions corresponding to the d^9, d^6, and d^5 configurations corresponding to Rh(0), Rh(III), and Rh(IV) (*31*). Contributions from each configuration were estimated by taking the integrated amplitudes of the Lorentzian peaks. The resulting best fits to the near edge spectra obtained for the treated catalyst samples were dominated by contribution of Rh(III), in all cases at least 90%. This comparison of the near edge structure indicates that the Rh oxide in the treated catalyst samples is dominated by Rh_2O_3 rather than Rh(0) or RhO_2.

The radial structure functions obtained for the same set of catalysts are shown in Fig. 3. A number of general trends can be observed in these functions. First, the radial structure functions (RSFs) suggest a crystallite domain size substantially smaller than that of the bulk form of Rh_2O_3, primarily because of the smaller intensities of the 2nd and third dominant shells in these functions.

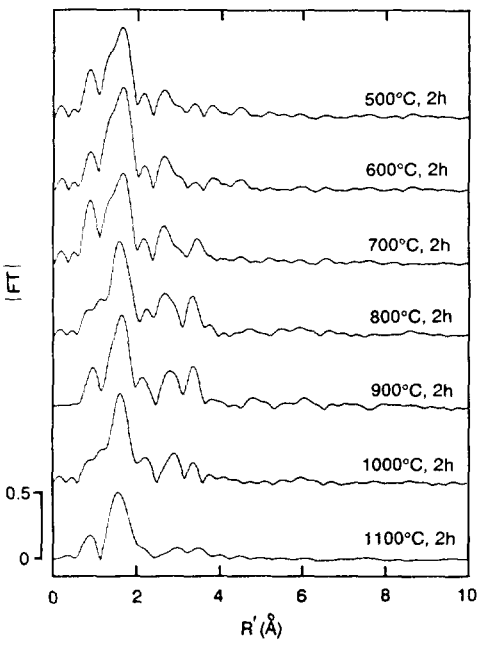

FIG. 3. Radial structure functions obtained for all catalyst samples treated in 5% O_2/N_2 for 2 h at various temperatures.

However, the dominant peaks in the RSFs occur at roughly similar radial distances as in bulk Rh_2O_3, again suggesting the Rh particles in the catalyst samples are dominated by this orthorhombic structure. Second, we qualitatively note that the intensities of the 2nd and 3rd dominant shells in the RSFs generally increase with increasing treatment temperature up to 800°C, but decrease with further increases in treatment temperature up 1100°C. Qualitatively, this trend can be interpreted as an increase in the size of the domains of crystalline Rh_2O_3 with increasing treatment temperature up to 800°C, but a decrease in the size of crystalline domains with further increasing treatment temperature up to 1100°C.

The dominant features in the RSFs were individually filtered and analyzed according to the procedure described in the Experiment section, and the resulting coordination numbers, mean radial distances, and mean square displacements obtained for this series of data are summarized in Table 2. The first or nearest neighbor shell in the treated catalyst samples was identified as an oxygen anion shell from the character of its phase and amplitude functions. The dependence of the amplitude function in particular on the atomic number has been well characterized and is discussed elsewhere (*25, 28–30*). This shell was analyzed using phase and amplitude functions extracted from the first oxygen anion shell in orthorhombic Rh_2O_3. For all samples, a single Gaussian shell (all scatterers in the shell are equally displaced from the central atom) was used in the fit. Attempts to fit the data using two or three gaussian shells with displacements more accurately reflecting the crystallographic structure of Rh_2O_3 resulted in marginal, if any, improvement in the fit, and was thus not used to obtain coordination and displacement information. Two higher order shells also dominated the RSFs of the treated catalyst samples. These shells consist mostly of a contribution from Rh(III) cations with some residual contribution from oxygen anions as we have discussed in an earlier section. Coordination values and mean radial displacements were also obtained for these shells using a single gaussian shell resulting in very good fits to the $\chi(k)$ functions above 3 $Å^{-1}$ for cases in which the resulting coordination number was greater than unity.

TABLE 2

Analysis of Individual Coordination Shells for Rh/Al_2O_3 Following Oxygen Aging at Various Temperatures

Treatment	Shell		N^a	R (Å)^b	$\Delta\sigma^2$
500°C, 2 h	1st	Rh–O	6.1	1.92	−0.001
	2nd	Rh–Rh	1.1	3.05	−0.001
	3rd	Rh–Rh	—	—	—
600°C, 2 h	1st	Rh–O	6.1	1.95	−0.002
	2nd	Rh–Rh	1.5	3.02	−0.003
	3rd	Rh–Rh	0.5	3.69	−0.003
700°C, 2 h	1st	Rh–O	6.2	1.97	−0.002
	2nd	Rh–Rh	2.2	3.01	−0.004
	3rd	Rh–Rh	1.2	3.68	−0.003
800°C, 2 h	1st	Rh–O	6.1	1.99	−0.002
	2nd	Rh–Rh	3.4	3.03	−0.005
	3rd	Rh–Rh	2.3	3.68	−0.004
900°C, 2 h	1st	Rh–O	6.2	2.00	−0.002
	2nd	Rh–Rh	1.6	2.96	−0.004
	3rd	Rh–Rh	2.6	3.68	−0.004
1000°C, 2 h	1st	Rh–O	5.1	2.00	−0.001
	2nd	Rh–Rh	1.6	3.11	−0.002
	3rd	Rh–Rh	1.1	3.79	−0.003
1100°C, 2 h	1st	Rh–O	2.1	1.9	−0.003
	2nd	Rh–Rh	1.1	3.13	−0.004
	3rd	Rh–Rh	0.8	3.80	−0.003
Rh Black	1st	Rh–O	6.3	2.05	−0.001
(900°C, 12 h)	2nd	Rh–Rh	3.9	3.01	−0.002
	3rd	Rh–Rh	8.9	3.65	−0.002

[a] Error was typically ±1.0 units for the 1st shell, ±0.5 units for the second shell, and ±1.0 units for the third shell.

[b] Error was typically ±0.02 units for the first shell, ±0.02 units for the second shell, and ±0.3 units for the third shell.

The structural parameters summarized in Table 2 are consistent with our qualitative observations about the behavior of the Rh_2O_3 crystal domain size as a function of treatment temperature. The coordination values for each of the three significant shells of the supported Rh oxide are shown in Fig. 4 as a function of treatment temperature and are consistent in following this trend. As the treatment temperature was increased from 500 to 800°C, the nearest neighbor oxygen anion shell remained fully sixfold coordinated, but the coordination in the two Rh(III) cation shells increased, consistent

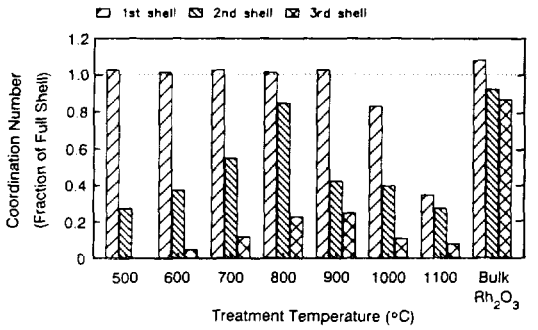

FIG. 4. Coordination numbers of the first three shells in the Rh_2O_3 structure obtained for all catalyst samples treated for 2 h in O_2/N_2. Values are expressed as the fraction of the full shell value.

with our earlier suggestion of an increase in the Rh_2O_3 crystal domain size. Note that the coordination number of the second shell (first Rh(III) cation shell) nearly reaches the bulk value of 4 following the 800°C treatment. The third shell (second Rh(III) cation shell) reaches a maximum value of 2.5, substantially lower than the bulk value of 10. The decrease in the domain size with increasing treatment temperature from 900 to 1100°C is dramatic. The loss of coordination in the Rh(III) cation shells and particularly in the nearest neighbor oxygen anion shell following treatment at 1000°C and higher is distinct from the behavior at low temperature where the closest oxygen anion shell remains fully coordinated. The comparison of the behavior of Rh/Al_2O_3 with the behavior of bulk Rh oxide in high temperature environments containing a partial pressure of oxygen provides some insight to explain this behavior. The behavior for bulk Rh oxide has been investigated as a function of temperature for various partial pressures of O_2 (*32, 33*). Focusing on the behavior of Rh oxide as the temperature is increased, one finds hexagonal Rh_2O_3 is thermodynamically favored between ~700 and ~900°C, while orthorhombic Rh_2O_3 is favored between ~900 and ~1030°C. Above this latter temperature, metallic Rh is favored. In this study, we found the supported noble metal in all of the treated catalysts to be fully oxidized and in a form similar to orthorhombic Rh_2O_3 polymorph. At present we believe the apparent decrease in the crystal domain size of the supported Rh oxide particles with treatment temperature above 900°C, and particularly the decrease in the coordination of the oxygen anion shell, to suggest a precursor to the formation of Rh metal, perhaps through a suboxide intermediate. The reason this transition appears to begin at a temperature below that observed for the bulk material (1030°C) is not known but may be related to the relatively low partial pressure of oxygen used in these experiments (5% of atmospheric pressure, or about 38 Torr). Note, however, that the oxidation state of the Rh does not appear to change significantly after treatment at these high temperatures, as indicated by the near-edge structure in Fig. 2, and no Rh(0)–Rh(0) metal shell is detectable. The possibility of the formation of isolated Rh atoms can also be discounted, since no evidence of a Rh(0)–oxygen anion shell was found. This type of oxygen anion shell has been observed in other studies of highly dispersed Rh/Al_2O_3 following treatment in hydrogen and is positioned at a radius of 2.68 to 2.71 Å from the central Rh(0) scatterer (*34, 35*).

The mean radii determined for the three main shells in the radial structure functions obtained for the treated catalysts (Table 2) are also of interest to compare with the bulk form of Rh_2O_3. Focussing on the first oxygen anion shell, note that the mean radial distance is in the range 1.99 to 2.01 Å for all of the catalyst samples. These displacements are shorter than the mean oxygen anion distance of 2.05 Å in hexagonal Rh_2O_3 and 2.06 Å in orthorhombic Rh_2O_3, but slightly longer than the distance of 1.96 Å in RhO_2. To check the validity of the shell analysis, the mean shell distance was also obtained using a sample of Rh black treated in flowing 5% O_2/N_2 at 900°C, which is known to produce large orthorhomic Rh_2O_3 crystallites from X-ray powder diffraction measurements. The mean radii of the oxygen anion shell obtained for the treated Rh

black was determined to be 2.05 Å, consistent with the crystallographic values determined for bulk Rh_2O_3. The observation of a contracted oxygen anion shell in the catalyst samples has also been observed for Rh/MgO, where it was attributed to a supported RhO_2 structure (*36*). Since the near-edge spectra for these treated catalysts do not resemble that of the RhO_2 reference compound (Fig. 2), but are more characteristic of Rh_2O_3, the relatively short first shell distance is not attributable to an oxide structure like RhO_2. At present we suggest that the relatively short displacement of the oxygen anion shell is related to a particle size effect. In all of the catalyst samples treated at or below 900°C, the nearest neighbor oxygen anion shells are fully coordinated. In small particles, this suggests that some of the oxygen anions are terminally bound on the surface of the Rh_2O_3 moiety, leading to a contracted Rh(III)–O displacement for these anions. Further studies of the particle size effect on bond distances are needed to better understand these observed shell contraction phenomena.

The second and third observed shells in all of the catalysts treated at 600°C and above were sufficiently intense to allow measurement of the mean radial distance. The mean radii of the second shell obtained for catalysts treated at a temperature of 900°C or lower ranged from 3.01 to 3.04 Å, in agreement with the value determined for the bulk form of Rh_2O_3, 3.03 Å. Analysis of the third shells obtained for samples treated at 600°C and above also yielded radii in general agreement with the corresponding shell in bulk Rh_2O_3. The resulting Debye–Waller factors, however, suggest a slightly greater degree of uniformity in the radii for the Rh_2O_3 domains in the treated catalysts than in the reference compound. When the catalyst was exposed to flowing oxygen at 1000 or 1100°C, however, the resulting radii of both Rh(III) cation shells were longer than the corresponding values obtained for the bulk Rh_2O_3. The error in the measurement of the radii is greater than normally encountered because of the low population of this shell ($N \sim 1$), but the increase in the measured radii is sufficiently large to be considered a real effect. This observation coincides with the dramatic loss of coordination in the first oxygen anion shell. We also note that the Debye–Waller factors determined for all shells in these latter two samples are generally higher than for those samples aged at lower temperatures. These observations point to a change in the structure of the supported Rh oxide from orthorhombic Rh_2O_3 to another form, as well as a decrease in the crystallite domain size.

Crystal domain size is not necessarily indicative of Rh_2O_3 particle size, due to the possibilities that particles may be amorphous in character, or if crystalline, they may have grain boundaries or twinned structures; thus, the value of using XAFS for obtaining Rh_2O_3 particle size is limited. However, the information provided by XAFS in elucidating the structural aspects of very small particles cannot be accessed by other techniques, such as powder X-ray diffraction, and in some cases, even by high-resolution TEM. The information provided by XAFS is also of value in providing information about the morphology of crystallites, and in particular, distinguishing between three-dimensional and two-dimensional crystallites. Therefore, we compared the coordination parameters of the three dominant shells obtained for the oxygen-aged Rh/Al_2O_3 catalysts with coordination parameters predicted by model Rh_2O_3 crystallites of varying size and morphology in order to estimate the mean crystallite domain size of the supported Rh oxide. These estimates are shown in Fig. 5 assuming three-dimensional (solid) crystallites (attempts to compare the catalyst data with two-dimensional crystallite models resulted in very poor fits). The domain size, represented in terms of the number of Rh(III) cations in the crystallite, increases with treatment temperature up to about 800°C, but then declines as the temperature increases further to 1100°C. At the maximum size, we estimate that a single

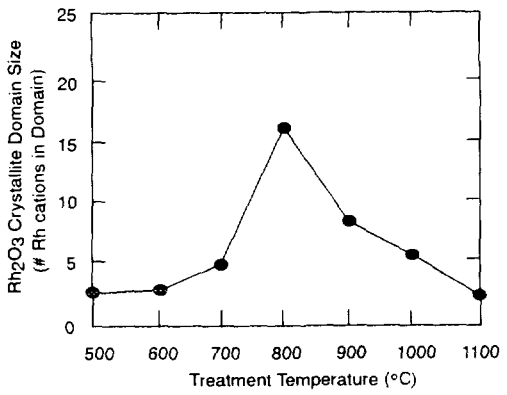

FIG. 5. Estimate of Rh_2O_3 mean crystallite domain size for all catalyst samples treated for 2 h in O_2/N_2. Basis of estimates are explained in the text.

Rh_2O_3 crystallite containing between 15 and 20 Rh(III) cations is on the order of 10 Å in diameter, assuming solid particles based on extension of the unit cell.

This behavior is in general consistent with the Rh_2O_3 structures observed in TiO_2-supported Rh particle oxidation studies using high resolution TEM (*37, 38*). In that study, the authors observed the formation of a Rh oxide shell which grows from the outside toward the core of the Rh metal particle. It was suggested that the oxide structure begins as a suboxide (RhO), progresses to a Rh_2O_3 structure, then forms multiply twinned or polycrystalline Rh_2O_3 crystal domains (*37, 38*). According to this model, crystal domains in the Rh_2O_3 particles would increase as Rh_2O_3 crystallites nucleate and grow, but as long as the particles remain polycrystalline, the ultimate domain size would be limited, consistent with our observation of domains which grow to a maximum of 10–20 Å. In a companion study, we will present results which further support this model.

For three selected treatment temperatures (600, 800, and 1000°C), several catalyst samples were aged, each for a different duration (1, 2, 4, and 15 h). As an example, the radial structure functions for catalyst samples aged at 800°C are shown in Fig. 6. The three dominant shells which appear in the radial structure functions of these treated samples were individually analyzed, and the structural parameters obtained from this analysis are summarized in Tables 3, 4, and 5. For treatment at 600°C, extended treatment results in a small increase in the coordination values of the 2nd and 3rd dominant shells (Table 3 and Fig. 7). The domain size of the Rh oxide increases only slightly, and even following the 15-h treatment, the crystal domains remain below the size of the Rh_2O_3 unit cell, as shown in Fig. 8. The relative lack of increase in domain size is consistent with growth of Rh_2O_3 species as a film, as suggested by Burkhardt and Schmidt for treatment of Rh/Al_2O_3 in oxygen at this temperature (*39*), although the XAFS data is not as conclusive as the direct TEM imaging method. For treatment at 800°C, note that the coordination numbers for the second and third shells increase dramatically with treatment time within the two hours of treatment, but further ordering proceeds at a slower rate (Table 4 and Fig. 7). The increase in the 2nd and 3rd shells

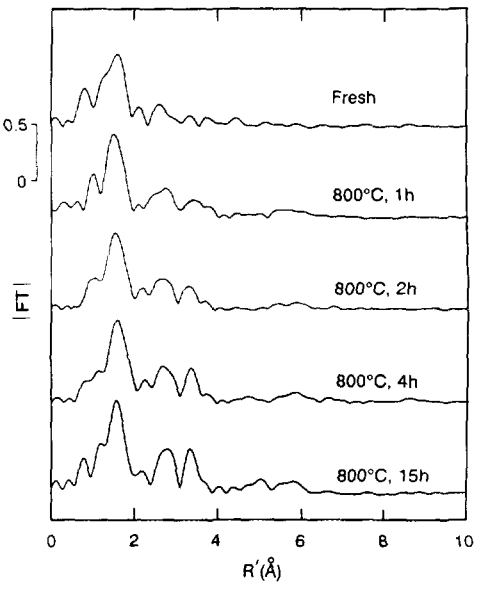

FIG. 6. Radial structure functions obtained for a fresh sample and catalyst samples treated at 800°C for various lengths of time.

TABLE 3

Analysis of Individual Coordination Shells for Rh/Al_2O_3 Following Oxygen Aging at 600°C for Various Times

Treatment	Shell		N^a	R (Å)^b	$\Delta\sigma^2$
Fresh	1st	Rh–O	6.2	1.92	−0.001
	2nd	Rh–Rh	1.1	3.05	−0.002
	3rd	Rh–Rh	—	—	—
600°C, 1 h	1st	Rh–O	6.1	1.95	−0.002
	2nd	Rh–Rh	1.3	3.06	−0.002
	3rd	Rh–Rh	—	—	—
600°C, 2 h	1st	Rh–O	6.0	1.94	−0.001
	2nd	Rh–Rh	1.5	3.04	−0.002
	3rd	Rh–Rh	—	—	—
600°C, 4 h	1st	Rh–O	6.0	1.95	−0.001
	2nd	Rh–Rh	1.5	3.03	−0.002
	3rd	Rh–Rh	—	—	—
600°C, 15 h	1st	Rh–O	6.2	1.94	−0.001
	2nd	Rh–Rh	1.8	3.04	−0.002
	3rd	Rh–Rh	0.8	3.67	−0.003

[a] Error was typically ±1.0 units for the 1st shell, ±0.5 units for the second shell, and ±0.5 units for the third shell.
[b] Error was typically ±0.03 units for the first shell, ±0.02 units for the second shell, and ±0.03 units for the third shell.

TABLE 4

Analysis of Individual Coordination Shells for Rh/Al_2O_3 Following Oxygen Aging at 800°C for Various Times

Treatment	Shell		N^a	R (Å)^b	$\delta\sigma^2$
Fresh	1st	Rh–O	6.2	1.92[b]	−0.001
	2nd	Rh–Rh	1.1	3.05	−0.002
	3rd	Rh–Rh	—	—	—
800°C, 1 h	1st	Rh–O	6.1	1.98	−0.002
	2nd	Rh–Rh	1.8	3.01	−0.002
	3rd	Rh–Rh	0.9	3.67	−0.003
800°C, 2 h	1st	Rh–O	6.1	1.99	−0.002
	2nd	Rh–Rh	3.4	3.03	−0.003
	3rd	Rh–Rh	2.3	3.68	−0.003
800°C, 4 h	1st	Rh–O	6.0	2.00	−0.003
	2nd	Rh–Rh	3.7	3.04	−0.003
	3rd	Rh–Rh	3.2	3.68	−0.004
800°C, 15 h	1st	Rh–O	5.3	2.00	−0.003
	2nd	Rh–Rh	3.9	3.05	−0.005
	3rd	Rh–Rh	3.5	3.68	−0.006

[a] Error was typically ±1.0 units for the 1st shell, ±0.5 units for the second shell, and ±0.5 units for the third shell.
[b] Error was typically ±0.03 units for the first shell, ±0.02 units for the second shell, and ±0.03 units for the third shell.

indicates the growth of solid Rh_2O_3 (rather than two-dimensional) crystallite domains, which also is in agreement with the findings by Burkhardt and Schmidt for Rh/Al_2O_3 treated in oxygen at temperatures higher than 600°C (*39*). The kinetic behavior of the growth of Rh oxide crystallites at 800°C is similar to that of the sintering growth of supported Rh metal particles when treated in a reducing environment (*16*). However, the crystal domain size of the Rh oxide particles treated in 5% O_2–N_2 is smaller (10 Å at the maximum) than the domain size reached by Rh metal particles (between 15 and 40 Å) characterized using the same catalysts treated for the same duration in 5% H_2/N_2 reducing environments at the same temperature. This conclusion is supported by the inability to detect Rh_2O_3 crystal domains for any of these treated samples using X-ray diffraction measurements. Figure 8 shows the estimated Rh_2O_3 crystallite domain size as a function of treatment time for the isothermal experiments. As in Fig. 5, the mean crystallite size was estimated by comparing the coordination parameters with those predicted using a solid structural model of

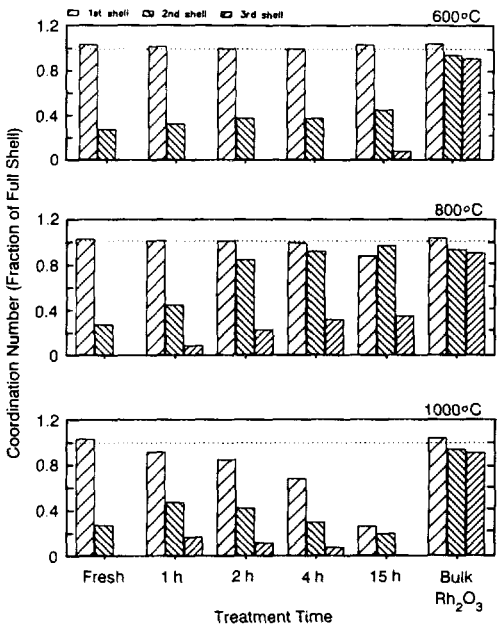

FIG. 7. Coordination numbers of the first three shells in the Rh_2O_3 structure for samples aged at 600, 800, and 1000°C as a function of treatment time. Values are expressed as the fraction of the full shell value.

TABLE 5

Analysis of Individual Coordination Shells for Rh/Al_2O_3 Following Oxygen Aging at 1000°C for Various Times

Treatment	Shell		N^a	R (Å)^b	$\delta\sigma^2$
Fresh	1st	Rh–O	6.2	1.92[b]	−0.001
	2nd	Rh–Rh	1.1	3.05	−0.002
	3rd	Rh–Rh	—	—	—
1000°C, 1 h	1st	Rh–O	5.5	2.00	−0.004
	2nd	Rh–Rh	1.9	3.08	−0.005
	3rd	Rh–Rh	1.7	3.71	−0.004
1000°C, 2 h	1st	Rh–O	5.1	2.00	−0.004
	2nd	Rh–Rh	1.7	3.12	−0.003
	3rd	Rh–Rh	1.1	3.79	−0.005
1000°C, 4 h	1st	Rh–O	4.1	1.99	−0.003
	2nd	Rh–Rh	1.2	3.13	−0.002
	3rd	Rh–Rh	0.7	3.80	−0.002
1000°C, 15h	1st	Rh–O	1.6	2.00	−0.001
	2nd	Rh–Rh	0.8	3.15	−0.001
	3rd	Rh–Rh	—	—	—

[a] Error was typically ±1.0 units for the 1st shell, ±0.5 units for the second shell, and ±0.5 units for the third shell.
[b] Error was typically ±0.3 units for the first shell, ±0.02 units for the second shell, and ±0.03 units for the third shell.

Rh_2O_3. The result of these estimates clearly indicate the growth of Rh_2O_3 crystallite domains with increasing treatment duration, but only to a maximum of approximately 10 to 15 Å in diameter. The ratio of the 2nd shell coordination to the 3rd shell coordination is consistent with three-dimensional (rather than two-dimensional) structure in these domains.

For treatment at 1000°C, extended treatment in 5% O_2/N_2 results in an initial increase in the coordination of the 2nd and 3rd shells, followed by a steady and continued decrease in the coordination number of all three dominant shells, as shown in Fig. 7 and listed in Table 5. Even the coordination of the nearest neighbor oxygen anions is significantly reduced after 2 h of treatment. Note also that the 2nd and 3rd shell radii increase as a function of time at this treatment temperature. Although not shown, the near edge structure of the catalysts treated for extended times compares more closely to Rh(III) than to Rh(IV) or Rh(0), although the quality of the fit using mostly d^6 character is poorer than for catalysts treated at lower temperatures. These observations suggest at extended treatment times, the Rh_2O_3 crystallite domains break down. Although this behavior could be explained by redispersion of the Rh oxide, we note that when catalysts are prepared in such a way as to yield very highly dispersed Rh oxide particles, the first shell is near full coordination. An alternative explanation for these observations involves a local structural transformation to a suboxide form with lower oxygen anion stoichiometry, such as RhO. The structure of this moiety may be poorly defined. We suggest the dramatic loss of oxygen anion coordination observed after 15 h may be indicative of the isolation of Rh species, which may preclude formation of Rh metal. We note from direct observation that bulk Rh_2O_3 treated in 5% O_2/N_2 for 15 h at 1000 and at 1100°C is converted to mostly Rh metal, suggesting that in the catalyst that a strong metal–support interaction kinetically hinders the transformation to form Rh metal. This form of Rh is difficult to reduce to the metallic form using 5% H_2/N_2, requiring a reducing treatment at a

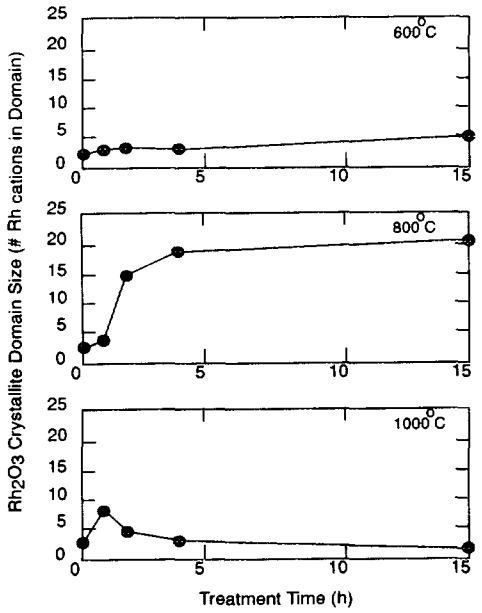

FIG. 8. Estimate of mean Rh_2O_3 domain size for a fresh sample, and for samples aged at 600, 800, and 1000°C as a function of treatment time.

temperature of at least 900°C. In contrast, supported Rh oxide produced by treatments in 5% O_2/N_2 at temperatures lower than 800°C can be easily converted to metal particles using reducing treatments below 500°C. Thus, it is possible that the unusual Rh oxide structures observed with extended treatment at 1000°C are involved in the oxidative deactivation of Rh which has been debated in the literature (*11–16*). The observation of an initial increase in Rh_2O_3 crystallite size, followed by a more gradual decrease in crystallite size together with loss of first shell coordination and expansion of the higher order shells suggests that the growth of Rh_2O_3 crystallites is kinetically fast in comparison to the transformation to this latter form of Rh, but the latter is thermodynamically favored at the treatment condition used.

As a final note, other researchers have advanced explanations for the oxidative deactivation of Rh on Al_2O_3 supports which involve reaction between Rh and the support (*24*), possibly forming a spinel-like structure on the surface or resulting in dissolution of Rh into the Al_2O_3 bulk, or which involve partial encapsulation of Rh by Al_2O_3. We conclude that for the conditions used in this study, it is unlikely that Rh deactivation involves formation of a spinel structure with Al_2O_3 or dissolution of Rh into the bulk, because the observations and analysis of the XAFS spectra are not consistent with these suggestions. Specifically, these models would involve coordination between Rh(III) cations and Al(III) cations at a radial distance of ~2.7 Å, assuming substitution of Rh(III) for Al(III) in the corundum Al_2O_3 structure, and although the coordination number may be relatively small (perhaps as low as 1), the intensity of the peak should be detectable, based on the predicted scattering cross-section of Rh(III)–Al(III) at a distance of 2.7 Å. None of the distinguishable shells in the XAFS spectra of the catalyst samples treated at the high temperatures had corresponding phase and amplitude functions consistent with Al cations (*30*), even if Al was taken to be a minor contribution to the shell, the balance of the contribution being from Rh(III) or oxygen. Therefore, we conclude that formation of a spinel with Al_2O_3 or dissolution into the Al_2O_3 bulk is not significant. Rather, we suggest deactivation of Rh in this environment involves an alternate mechanism involving a strong interaction between the Rh_2O_3 species and the support. The results obtained in this study do not conclusively show evidence for partial encapsulation or decoration of Rh by the support, but it is not inconsistent with such a rationalization. Evidence for this behavior has been observed for Rh metal supported on an Al_2O_3 thin film and treated in vacuum at high temperature (*40*).

SUMMARY

In summary, the XAFS technique has been used to characterize changes in the local structure of Rh oxide and/or Rh metal particles supported on alumina caused by treatment in oxygen at various elevated temperatures in the range 500 to 1100°C. A qualitative comparison of the near edge spectra and of the individual shells in the radial distribution function reveals that in these catalysts, Rh is completely oxidized to Rh_2O_3 following treatment at or above 500°C. The Rh oxide particles clearly have a structure similar to orthorhombic Rh_2O_3. The crystallite domain size increases with treatment temperature, reaching a maximum of ~10–20 Å at 800°C. Above a treatment temperature of 900°C, the local structure around Rh changes in such a way as to suggest a change in the structure from orthorhombic Rh_2O_3 to a less well defined structure which is noncrystalline and has lower oxygen coordination, such as RhO moieties suggested by Dayte and co-workers (*37, 38*) and which is thermodynamically favored under these conditions. Evidence for formation of spinel structures involving Rh(III) and Al(III) or dissolution of Rh into the Al_2O_3 bulk was not found. However, our results are consistent with a strong metal-support interaction which inhibits sintering or growth of large

Rh_2O_3 crystallites at temperatures below 900°C, and which inhibits formation of Rh metal predicted by the phase behavior at temperatures above 1000°C. Further study is needed to better characterize the nature of this interaction and its effect on the activity of these catalysts.

ACKNOWLEDGMENTS

The authors thank M. J. D'Aniello and M. Zammit for preparing the catalyst samples, and J. L. Johnson for performing X-ray diffraction measurements of the reference compounds and thermally treated catalyst samples. The authors also thank Professor R. W. Hoffman of Case Western Reserve University for his helpful comments. Finally, the authors acknowledge the NSLS staff for their support during these experiments, and in particular J. Scrafani and L. Fareria for their assistance at beamline X-11A. Research performed at NSLS is supported in part by the United States Department of Energy, Division of Materials Sciences and Division of Chemical Sciences.

REFERENCES

1. Taylor, K. C., "Automobile Catalytic Converters," Springer-Verlag, Berlin, 1984.
2. Schlatter, J. C., and Taylor, K. C., *J. Catal.* **49,** 42 (1977).
3. Taylor, K. C., *Ind. Eng. Chem. Prod. Res. Dev.* **11,** 54 (1972).
4. Hughes, R., "Deactivation of Catalysts," Academic Press, London, 1984.
5. Ruckenstein, E., *in* "Metal–Support Interactions in Catalysis, Sintering, and Redispersion" (S. Stevenson, J. A. Dumesic, R. T. K. Baker, and E. Ruckenstein, Eds.), p. 141. Van Nostrand–Reinhold, New York, 1987.
6. Wanke, S. E., and Flynn, P. C., *Catal. Rev.-Sci. Eng.* **12,** 93 (1975).
7. Bond, G. C., *Surf. Sci.* **156,** 966 (1985).
8. Koberstein, E., SAE Paper No. 770366, 1977.
9. Summers, J. C., and Ausen, S. A., *J. Catal.* **58,** 131 (1979).
10. Wong, C., and McCabe, R. W., *J. Catal.* **107,** 535 (1987).
11. Solymosi, F., and Pasztor, M., *J. Phys. Chem.* **90,** 5312 (1986).
12. Zaki, M. I., Kunzmann, G., Gates, B. C., and Knozinger, H., *J. Phys. Chem.* **91,** 1486 (1987).
13. Fuentes, S., and Figueras, F., *J. Catal.* **61,** 443 (1980).
14. Yates, D. J. C., Murrell, L. L., and Prestridge, R. B., *J. Catal.* **57,** 41 (1979).
15. Yates, D. J. C., and Prestridge, R. B., *J. Catal.* **106,** 549 (1987).
16. Beck, D. D., and Carr, C. J., *J. Catal.* **144,** 296 (1993).
17. Wong, C., and McCabe, R. W., *J. Catal.* **119,** 47 (1989).
18. Bayer, G., and Wiedermann, H. G., *Thermochem. Acta* **15,** 213 (1976).
19. Beck, D. D., and Carr, C. J., submitted for publication.
20. Fiedorow, R. M. J., Chahar, B. S., and Wanke, S. E., *J. Catal.* **51,** 193 (1978).
21. Kiss, J. T., and Gonzalez, R. D., *Ind. Eng. Chem. Prod. Res. Dev.* **24,** 216 (1985).
22. Duprez, D., Delahy, G., Abderrahim, H., and Grimblot, J., *J. Chim. Phys.* **83,** 465 (1986).
23. Vis, J. C., van't Blik, H. F. J., Huizinga, T., van Grondelle, J., and Prins, R., *J. Catal.* **95,** 333 (1985).
24. Yao, H. C., Japar, S., and Shelef, M., *J. Catal.* **50,** 407 (1977).
25. Teo, B. K., *in* "EXAFS Spectroscopy: Techniques and Applications" (B. K. Teo and P. C. Joy, Eds.). Plenum Press, New York, 1981.
26. van Zon, J. B. A. D., Koningsberger, D. C., van't Blik, H. F. J., and Sayers, D. E., *J. Chem. Phys.* **82,** 5742 (1985).
27. Brown, G. S., and Doniach, S., *in* "Synchrotron Radiation Research" (H. Winick and S. Doniach, Eds.), p. 374. Plenum Press, New York, 1980.
28. Teo, B. K., and Lee, P. A., *J. Am. Chem. Soc.* **101,** 2815 (1979).
29. Teo, B. K., "EXAFS: Basic Principles and Data Analysis," Inorganic Chemistry Concepts, Vol. 9. Springer-Verlag, New York, 1986.
30. McKale, A. G., Veal, B. W., Paulikas, A. P., Chan, S.-K., and Knapp, G. S., *J. Am. Chem. Soc.* **110,** 3763 (1988).
31. Beck, D. D., Capehart, T. W., and Hoffman, R. W., *Chem. Phys. Lett.* **159,** 207 (1989).
32. Muller, O., and Roy, R., *J. Less-Common Met.* **16,** 129 (1968).
33. Schmahl, N. G., and Minzl, E., *Z. Phys. Chem. N. F.* **41,** 78 (1964).
34. Koningsberger, D. C., van Zon, J. B. A. D., van't Blik, H. F. J., Visser, G. J., Prins, R., Mansour, A. N., Sayers, D. E., Short, D. R., and Katzer, J. R., *J. Phys. Chem.* **89,** 4075 (1985).
35. van Zon, J. B. A. D., Koningsberger, D. C., Sayers, D. E., van't Blik, H. F. J., and Prins, R., *J. Chem. Phys.* **80,** 3914 (1984).
36. Emrich, R. A., Mansour, A. N., Sayers, D. E., McMillan, S. T., and Katzer, J. R., *J. Phys. Chem.* **89,** 4261 (1985).
37. Logan, A. D., Braunschweig, E. J., and Datye, A. K., *Ultramicroscopy* **31,** 132 (1989).
38. Logan, A. D., Sharoudi, K., and Datye, A. K., *J. Phys. Chem.* **95,** 5568 (1991).
39. Burkhardt, J., and Schmidt, L. D., *J. Catal.* **116,** 240 (1989).

40. Chen, J. G., Colaianni, M. L., Yates, J. T., Jr., and Fisher, G. B., *J. Phys. Chem.* **94,** 5059 (1990).
41. Wykoff, R. W. G., "Crystal Structures," 2nd ed., Vol. 1, p. 10, Wiley, New York, 1963.
42. Shannon, R. D., *Solid State Commun.* **6,** 139 (1968).
43. Coey, J. M., *Sect. B* **26,** 1876 (1970).
44. Poeppelmeier, K. R., Newsam, J. M., and Brown, J. M., *J. Solid State Chem.* **60,** 68 (1985).
45. Biesterbos, J. W. M., and Hornstra, J., *J. Less-Common Met.* **30,** 121 (1973).
46. Wold, A., Arnott, R. J., and Croft, W. J., *Inorg. Chem.* **2,** 972 (1963).